ARMY RESEARCH LABORATORY

Navier-Stokes Computations of Sabot Discard Using Chimera Scheme

by E. Ferry, J. Sahu,
and K. Heavey

ARL-TR-1524 October 1997

The findings in this report are not to be construed as an official Department of the Army position unless so designated by other authorized documents.

Citation of manufacturer's or trade names does not constitute an official endorsement or approval of the use thereof.

Destroy this report when it is no longer needed. Do not return it to the originator.

Army Research Laboratory
Aberdeen Proving Ground, MD 21005-5066

ARL-TR-1524 **October 1997**

Navier-Stokes Computations of Sabot Discard Using Chimera Scheme

E. Ferry, J. Sahu, K. Heavey
Weapons and Materials Research Directorate, ARL

Abstract

Computational fluid dynamics calculations have been performed for a multibody system consisting of a main projectile and three sabot components. Numerical flow field computations have been made for various orientations and locations of sabots using an unsteady, zonal Navier-Stokes code and the Chimera composite grid discretization technique at $M_\infty = 4.0$ and $\alpha = 0°$. Computational grids have been obtained for the projectile and sabot independently and then overset to form the complete grid system. Computed results have been obtained for sabot angles of attack of 5, 10, 15, and 25°. Computed results show the details of the expected flow field features including the shock interactions. Both laminar and turbulent computations for the 25° case predict similar results. Computed results for other sabot positions are compared with the experimental data obtained in Canada for the same configuration and conditions and are generally found to be in good agreement with the data.

Table of Contents

INTENTIONALLY LEFT BLANK.

List of Figures

INTENTIONALLY LEFT BLANK.

1. Introduction

During the gun-launch process of modern fin-stabilized kinetic energy projectiles, sabots are utilized to reduce in-bore balloting and smoothly carry the projectiles in the gun tube. Once free of the gun tube, the sabot components must be discarded to reduce the drag of the round. Good sabot separation is important to obtain a repeatable launch and flight of the projectiles. It has been demonstrated [1] that aerodynamic interference during the launch process can adversely affect the projectile trajectory and increase on-target dispersion. Mechanical interference during the sabot separation can also alter the projectile trajectory and may lead to unacceptable loss of accuracy at the target. The aerodynamic interference of the projectile and sabot flow field is quite complex (see Figure 1) and involves three-dimensional (3-D) shock/boundary layer interactions and separated flow regions. The sabot separation in actual flights can be asymmetrical which can further magnify the interference effects.

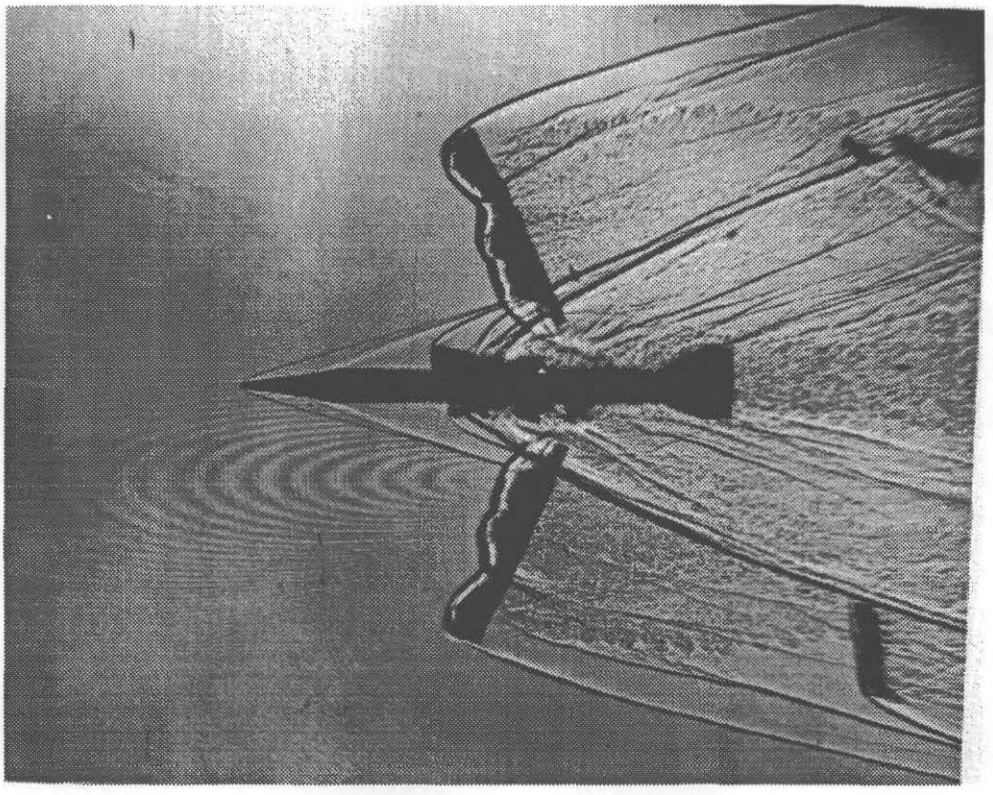

Figure 1. Spark Shadowgraph for a Projectile-Sabot System.

The sabot discard aerodynamics have been studied both theoretically and experimentally over the past few decades. Initial analytical modeling efforts [2] were empirical and based on Newtonian flow approximations. Although not general, this technique accurately modeled the flow in some cases. A more recent extension [3] of this modeling effort included an integrated flow element approach that utilized local shock/expansion procedures based on actual experimentally measured sabot surface pressures. Again, these analytical modeling techniques have their limitations, and in general, these theories cannot completely represent the complex flow fields associated with the interaction of the projectile and sabot flow fields.

An extensive experimental program [4,5] was carried out in 1981 to study the aerodynamics of sabot discard. Surface pressures were obtained experimentally on a generic configuration consisting of a projectile and three sabot components. The experimental test results showed regions of shock/boundary-layer interactions and separated flow regions. Recently, another experimental study [6] was conducted that included detailed pressure measurements on a generic cone-cylinder projectile as well as a full-scale model of the C-76 projectile. The generic configuration was chosen to provide calibration for computational fluid dynamics (CFD) modeling efforts. As pointed out earlier, the projectile and sabot interacting flow field is quite complex with 3-D shock/boundary-layer interactions and regions of separated flow. The CFD modeling technique is an emerging tool which can account for these 3-D interactions. Recent papers [6-8] show a rise in the use of CFD to accurately predict such flow fields. Often, the computed results are found to be in good agreement with the experimental data. These computational studies have provided enhanced understanding of the complex interacting flow fields; however, they used a steady-state approach. Research presented in this report emphasizes the use of an advanced CFD capability that can compute both steady-state and time-dependent sabot discard aerodynamics.

The advanced CFD capability used here solves the Navier-Stokes equations [9] and incorporates the Chimera technique [10–13]. The Chimera technique involves generating independent grids about each component and then oversetting them onto a base grid to form the complete model. With this composite overset grid approach, it is possible to use different grid topologies for the projectile and the sabot components, respectively. A complete model of the multibody system is thus made, and

the sabot discard aerodynamics can then be determined. Numerical flow field computations have been made for the projectile and sabot multibody system at a supersonic speed for symmetric sabot discard. Computed results have been compared with the experimental data [6] obtained for the same configuration and flow conditions.

2. Solution Technique

2.1 Governing Equations. The complete set of 3-D, time-dependent, generalized geometry, Reynolds-averaged, thin-layer Navier-Stokes equations is solved numerically to obtain a solution to this problem and can be written in general spatial coordinates ξ, η, and ζ as follows [14]:

$$\partial_\tau \hat{q} + \partial_\xi \hat{F} + \partial_\eta \hat{G} + \partial_\zeta \hat{H} = Re^{-1} \partial_\zeta \hat{S}, \tag{1}$$

In Equation 1, $\hat{q}$ contains the dependent variables: density, three velocity components, and energy. The thin-layer approximation is used here, and the viscous terms involving velocity gradients in both the longitudinal and circumferential directions are neglected. The viscous terms are retained in the normal direction, ζ, and are collected into the vector $\hat{S}$. These viscous terms are used everywhere.

2.2 Numerical Technique. The implicit, approximately factored scheme for the thin-layer Navier-Stokes equations using central differencing in the η and ζ directions and upwinding in ξ is written in the following form [14]:

$$\begin{aligned}
&\left[I + h\delta_\xi^b(\hat{A}^+)^n + h\delta_\zeta \hat{C}^n - hRe^{-1}\bar{\delta}_\zeta J^{-1}\hat{M}^n J - D_i|_\zeta\right] \\
&\times [I + h\delta_\xi^f(\hat{A}^-)^n + h\delta_\eta \hat{B}^n - D_i|_\eta]\,\Delta\hat{Q}^n \\
&= -\Delta t\{\delta_\xi^b[(\hat{F}^+)^n - \hat{F}_\infty^+] + \delta_\xi^f[(\hat{F}^-)^n - \hat{F}_\infty^-] + \delta_\eta(\hat{G}^n - \hat{G}_\infty) \\
&+ \delta_\zeta(\hat{H}^n - \hat{H}_\infty) - Re^{-1}\bar{\delta}_\zeta(\hat{S}^n - \hat{S}_\infty)\} - D_e(\hat{Q}^n - \hat{Q}_\infty),
\end{aligned} \tag{2}$$

where $h = \Delta t$ or $(\Delta t)/2$ and the free-stream base solution is used. Here, δ is typically a three-point second-order accurate central difference operator, $\bar{\delta}$ is a midpoint operator used with the viscous terms, and the operators δ_ξ^b and δ_ξ^f are backward and forward three-point difference operators. The flux $\hat{F}$ has been eigensplit, and the matrices $\hat{A}$, $\hat{B}$, $\hat{C}$, and $\hat{M}$ result from local linearization of the fluxes about the previous time level. Here, J denotes the Jacobian of the coordinate transformation. Dissipation operators D_e and D_i are used in the central space differencing directions.

2.3 Chimera Composite Grid Technique. The Chimera overset grid scheme is a domain decomposition approach where a full configuration is meshed using a collection of independent overset grids. This allows each component of the configuration to be gridded separately and overset into a main grid. Overset grids are not required to join in any special way. Usually, a major grid covers the entire domain or a grid is generated about a dominant body section. Minor grids are generated about the rest of the bodies or sections. Because each component grid is generated independently, portions of one grid may be found to lie within a solid boundary contained within another grid. Such points lie outside the computational domain and are excluded from the solution process. Equation 2 has been modified for Chimera overset grids by the introduction of the flag i_b to achieve just that. This i_b array accommodates the possibility of having arbitrary holes in the grid. The i_b array is defined such that $i_b = 1$ at normal grid points and $i_b = 0$ at hole points. Thus, when $i_b = 1$, Equation 2 becomes the standard scheme. But, when $i_b = 0$, the algorithm reduces to $\Delta\hat{Q}^n = 0$ or $\hat{Q}^{n+1} = \hat{Q}^n$, leaving $\hat{Q}$ unchanged at hole points. The set of grid points that form the border between the hole points and the normal field points are called intergrid boundary points. These points are updated by interpolating the solution from the overset grid that created the hole. Values of the i_b array and the interpolation coefficients needed for this update are provided by a separate algorithm [10]. The Chimera procedure reduces a complex problem into a number of simpler subproblems. Computations are performed on each grid separately. The grids are developed to use the available core memory one grid at a time. The remaining grids are stored on an external disk storage device such as the solid-state disk (SSD) device of the Cray Y-MP computer. A major part of the Chimera overset grid approach is the information transfer from one grid into another by means of the intergrid boundary points.

2.4 Boundary Conditions. For simplicity, most of the boundary conditions have been imposed explicitly [9]. An adiabatic wall boundary condition is used on the body surface, and the no-slip boundary condition is used at the wall. The pressure at the wall is calculated by solving a combined momentum equation. Free-stream boundary conditions are used at the inflow boundary as well as at the outer boundary. A symmetry boundary condition is imposed at the circumferential edges of the grid, while a simple extrapolation is used at the downstream boundary. A combination of symmetry and extrapolation boundary condition is used at the center line (axis). Since the free-stream flow is supersonic, a nonreflection boundary condition is used at the outer boundary. The outer boundary of the sabot grid completely lies within the background projectile grid and, thus, gets its flow field information interpolated from the projectile grid.

3. Model Geometry and Computational Grid

An advantage of the Chimera technique is that it allows computational grids to be obtained for each body component separately and, thus, makes the grid generation process easier. Figure 2 shows a computational grid for the complete model, including the projectile and sabot. This grid corresponds to the sabot angle of attack of 25°. The projectile grid consists of two zones (zone 1 and zone 2) that include a small zone (zone 1) in front of the projectile nose. Each of these two zones is a rectangular grid. The grid around the sabot also consists of two zones (zone 3 and zone 4) and was obtained using an O-topology and a rectangular topology, respectively. Figure 2 also shows the sabot grid (zone 3). The sabot grids were individually generated and then overset as shown in this figure to form the complete grid system. The computational grids shown here correspond to the pitch plane. The zone 2 projectile grid serves as the main background grid for the computation. The grid in zone 3 is an O-grid around the sabot petal. The grid in zone 4 sits along the edge of the sabot petal (not shown in this figure). Figure 3 shows a computational grid for computations with the sabot petal at angle of attack of 10°. Again, the same sabot grids are used here for this run, and there was no need to regenerate new sabot grids. The same sabot grids were also used for two other cases, which correspond to sabot angles of attack of 5° and 15°. In each case, the dimensions of different zones are as follows: zone 1, 16x32x80; zone 2, 86x32x80; zone 3, 72x32x30; and zone 4,

60x20x40. The entire grid system consisted of 378,240 grid points. Note that the grid setup allows computation of the base region flow field of the sabots. Grid points are clustered near the projectile and the sabot surfaces to capture the viscous boundary layers. No attempt has been made to adapt the computational grids to gradients in the flow field variables.

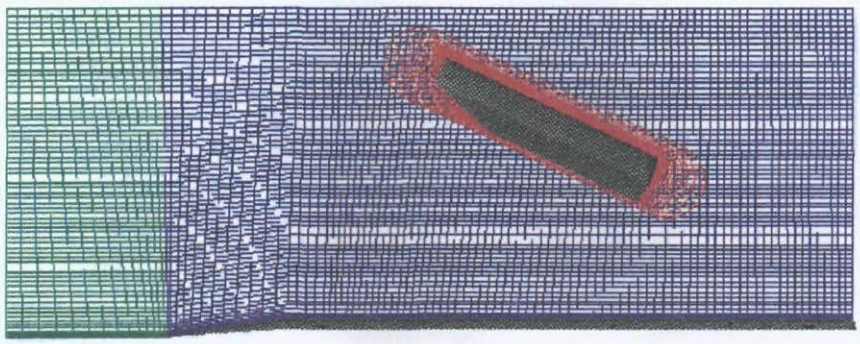

Figure 2. Computational Grid, Sabot Angle of Attack = 25°.

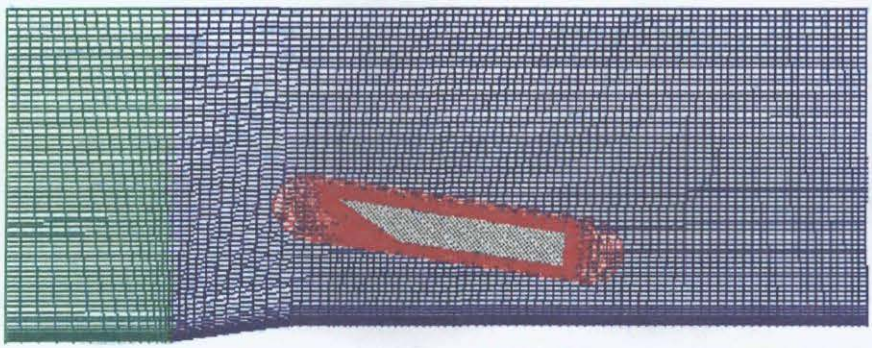

Figure 3. Computational Grid, Sabot Angle of Attack = 10°.

4. Results

Steady-state numerical calculations have been performed to numerically simulate the projectile and the sabot system. All computations have been run at $M_\infty = 4.0$ and for the same test conditions corresponding to the Canadian experiments [6]. Computational modeling is restricted to the symmetric sabot discard. Here, the projectile is at zero degrees angle of attack and three sabots are

discarded symmetrically following the same radial trajectory away from the projectile. Figure 4 shows a schematic diagram of the projectile and the sabot system. Since symmetric sabot discard is of interest here, the computational domain consists of a 60° segment, as shown in Figure 4. Also shown is the sabot grid, which is entirely contained in the background projectile grid. Because of symmetry, the requirements for grid sizes, computer resources such as computer memory, and run time are reduced.

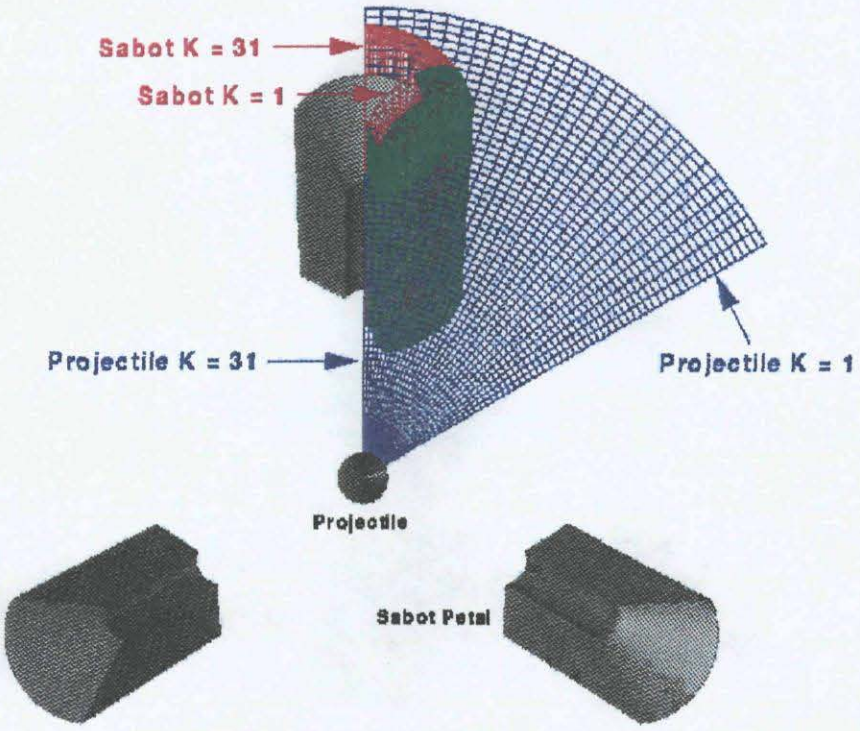

Figure 4. Schematic Diagram Showing the Computational Domain

Initially, a converged result for the sabot at 25° angle of attack was obtained. Figure 5 shows the computed Mach contours for this case. It shows the computed Mach contours for a circumferential cross-sectional plane which cuts through the projectile and the sabots. Although

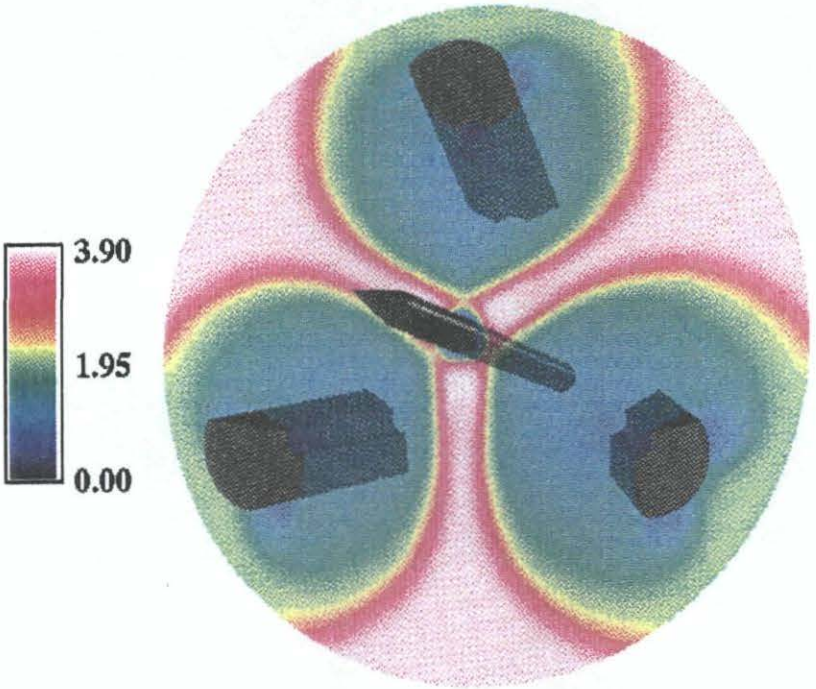

Figure 5. Shock Interactions in the Cross-Sectional Plane (Projectile and Sabots).

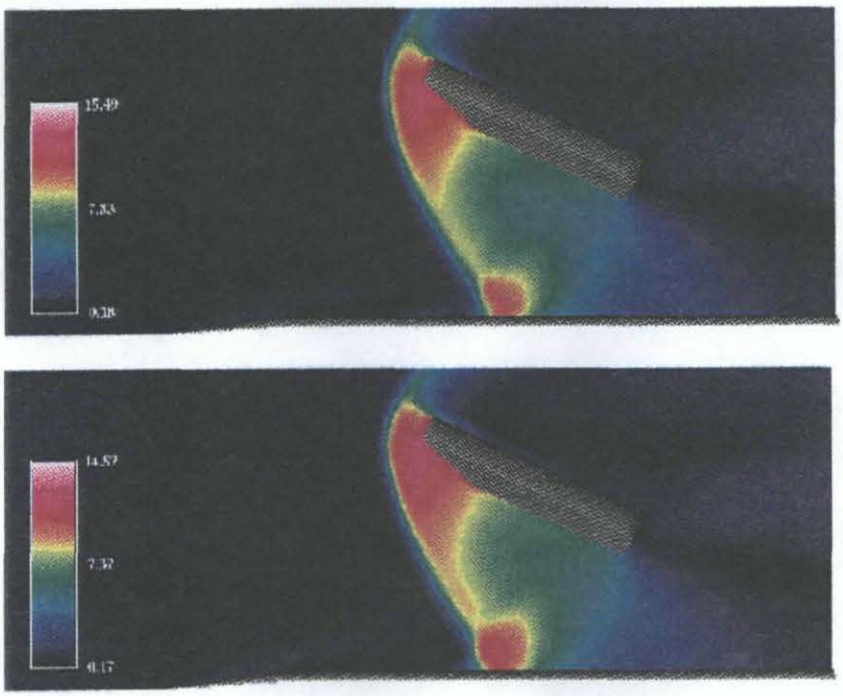

Figure 6. Computed Pressure Contours, M = 4.0, Sabot Angle of Attack = 25°, Laminar and Turbulent Solutions.

computations are performed only for a 60° sector due to symmetry, the computed results are shown here for the entire projectile and the sabot system. This figure clearly shows the shock interactions associated with the projectile and the sabot system. Figure 6 shows the computed pressure contours for the 25° sabot angle of attack case in the pitch plane. Both laminar and turbulent computations were performed and only small differences were observed between these results, especially near the sabot shock impingement point on the projectile. The turbulent calculations show slightly larger regions of shock-boundary layer interactions. The wind tunnel data for this case, however, was later found to have suffered from the wall blockage effects, and thus, numerical results for this case were not compared with the data. It shows an oblique shock wave emanating from the nose of the projectile and a detached bow shock in front of the sabot petal. The interactions of the projectile and the sabot flow fields can be seen clearly. Downstream of the shock-interaction point, a region of high pressure and low velocity exists. Based on the shock strengths, this interacting flow region may include regions of flow separation in addition to shock-boundary layer interactions. The computed result shown corresponds to the symmetry plane. A nonreflection outer boundary is used, which allows the outer boundary of the background computational grids to be placed near the sabots.

The next set of computed results corresponds to the B5, B10, and B15 cases. These three cases correspond to sabot angles of attack of 5°, 10°, and 15°. The projectile is at zero degrees angle of attack for all these cases. As stated earlier, the background grid for the projectile remains the same. The sabot grids again are the same but have been moved to the new positions and orientations. Figure 7 shows the pressure contours for the projectile and sabot in the symmetry plane. Computed results here have been obtained for the turbulent flow condition using an algebraic turbulence model. Similar to the 25° sabot angle of attack case, a nonreflection outer boundary is used, which allows the outer boundary of the background computational grids to be placed near the sabots. This figure clearly shows the interactions of the projectile and the sabot flow fields occurring at different longitudinal locations along the projectile. The computed pressure contours show the sabot shock impinging and reflecting off the projectile surface. This shock impingement results in a higher pressure region on the projectile surface just downstream of the impingement point. A high pressure region can also be observed behind the sabot shock. As expected, the flow behind the base region of the sabot is a low-pressure region. As the sabot angle of attack is increased, the sabot shock

impingement point on the projectile is moved further downstream. For the 5° sabot angle of attack, the sabot shock impinges on the projectile, reflects from the projectile surface, and impinges back on the sabot. The reflected shock from the projectile surface is seen to just miss the base of the sabot for the 10° sabot angle of attack case and is even further away from the sabot base at 15° sabot angle of attack. The flow field in the base region of the sabot is also seen to change considerably with an increase in sabot angle of attack.

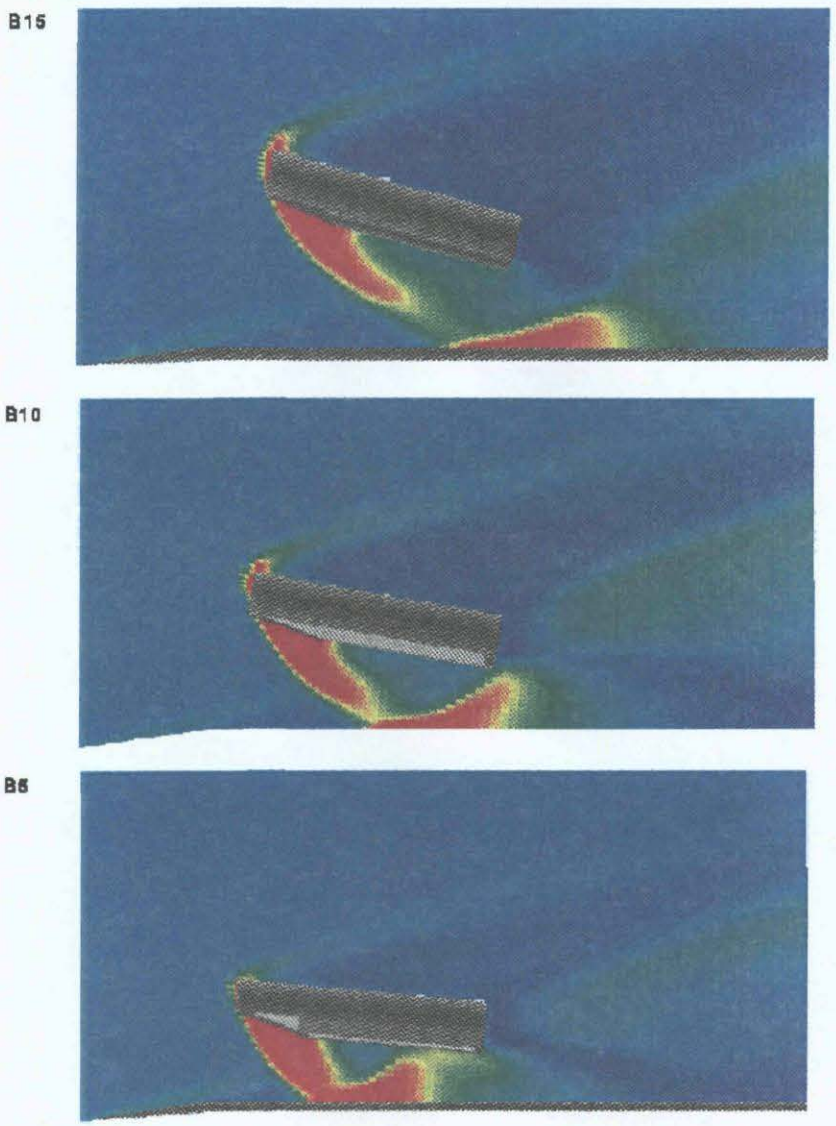

Figure 7. Computed Pressure Contours at Different Sabot Angles of Attack, 5°, 10°, and 15°, M = 4.0.

Figures 8 and 9 show the computed surface pressures, p/p_∞, for the sabot and the projectile, respectively. Here, X/D = 0.0 corresponds to the nose of the projectile. These computed surface pressures correspond to the pitch plane and are compared with the experimental data [6]. The computed pressures on the bottom surface of the sabot are shown in Figure 8 and are generally in good agreement with the experimental data. Some discrepancies do exist in the comparison of sabot surface pressure for the 5° angle of attack case. Due to close proximity of the sabot to the projectile, the flow field is, as expected, more complicated and includes complex shock-shock and shock-boundary layer interactions. Accurate computation of the resulting flow field is thus more difficult. Grid clustering/alignment in the nose region of the sabot may be needed to improve the accuracy of the numerical solution for this case. Similar experience has been noted by other researchers [6]. For X/D > 7, the agreement of the computed surface pressures with the data is very good even for the 5° angle of attack case. For this case, there is a secondary pressure rise near X/D = 11, which results from the reflected shock impinging on the underside of the sabot. This predicted pressure rise matches very well with the experimental data. As the sabot angle of attack is increased, the secondary pressure rise is reduced until it is eliminated at the 15° sabot angle of attack. The agreement of the computed sabot surface pressures with the data is good at angle of attack of 10° and 15°. Figure 9 shows the surface pressure distributions on the projectile in the pitch plane. Computed results are shown in solid line and are compared with the experimental data shown in dark circles for 5°, 10°, and 15° degree sabot angles of attack. As seen in this figure, the surface pressure is almost constant on the nose, which is followed by a pressure drop at the cone-cylinder junction. This computed pressure drop at the cone-cylinder junction agrees well with the data at the 15° sabot angle of attack; however, at lower angles of attack, the agreement is not so good. The predicted flow on the nose of the projectile corresponds to an undisturbed flow upstream of the shock impingement point. Clearly, the numerical results do not show the same extent of shock-boundary layer interactions observed experimentally. Similar results are also seen in the DREV CFD predictions [6]. A large pressure increase due to shock wave impinging on the projectile surface is seen in both computed and experimental data. The locations of the pressure peaks have been predicted correctly and agree well with the data. The magnitudes of the peak are, however, slightly underpredicted. Additionally, a secondary small peak is observed in the experimentally obtained surface pressure near X/D = 11 for the 5° case, which is not seen in the computed surface pressures.

It may be possible to improve the accuracy of the computed results either through grid refinement and/or use of advanced turbulence modeling, but further analysis has been limited due to time constraints.

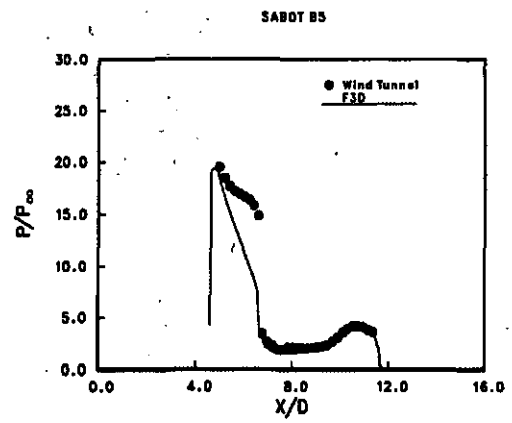

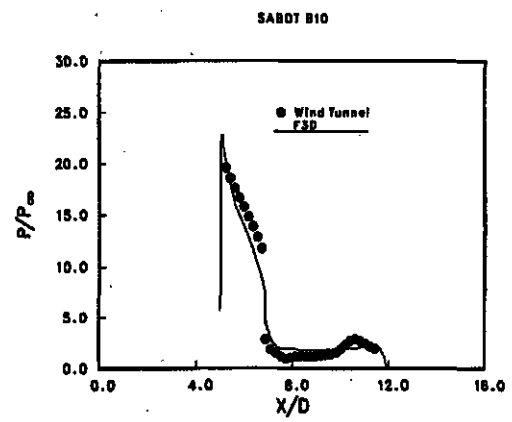

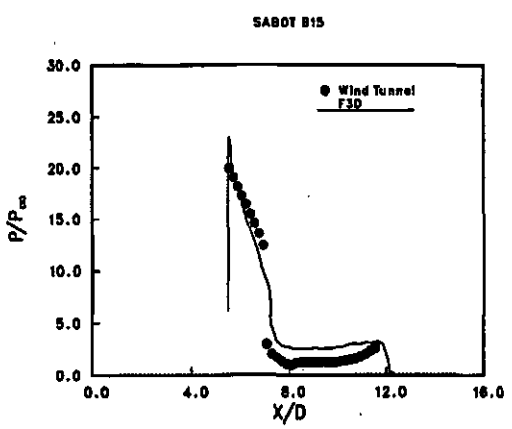

Figure 8. Sabot Surface Pressure Distributions.

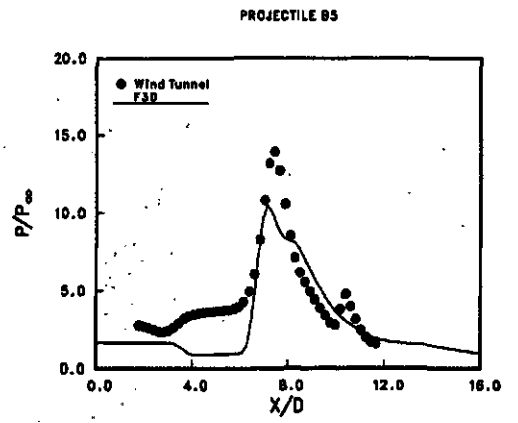

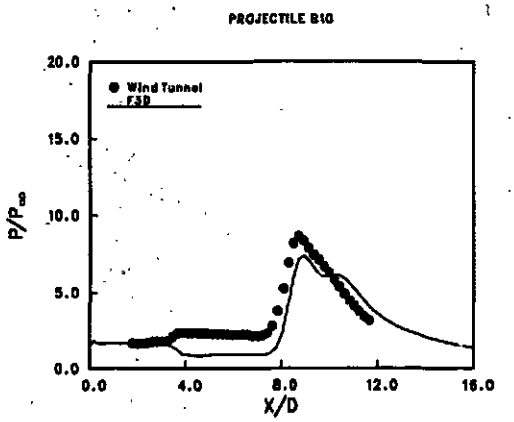

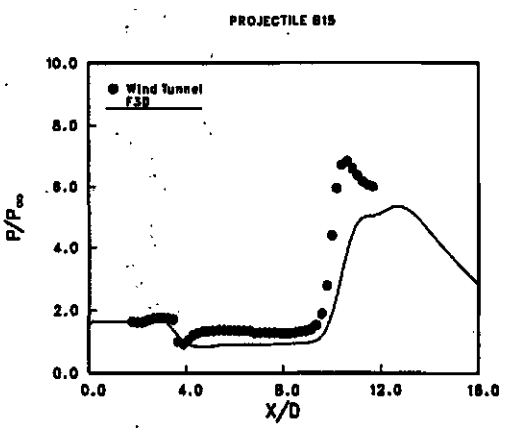

Figure 9. Projectile Surface Pressure Distributions.

5. Concluding Remarks

A computational study was undertaken to compute the 3-D flow fields for a multibody system consisting of a projectile and sabots. Flow computations were performed at a supersonic Mach number, $M_\infty = 4.0$ and $\alpha = 0.0°$ using a 3-D unsteady Navier-Stokes code and Chimera composite grid discretization technique. Overset body conforming grids were used to individually model the projectile and the sabot components. Computed results have been obtained for sabot angles of attack of 5°, 10°, 15° and 25°. Computed results show the qualitative features of the complex shock interaction flow field for the projectile and the sabots. Both laminar and turbulent computed results have been obtained for the 25° case, and the computed results do not show appreciable change in the surface pressures. Computed results for this case have not been compared with the experimental results due to blockage effects encountered in the tests. Computed results for the other three sabot positions are compared with the experimental data obtained at DREV, Canada, for the same configuration and conditions and are generally found to be in good agreement with the data. In some cases, discrepancies exist between the computed surface pressures and experimental data. Grid refinement and use of advanced turbulence modeling may be needed to further improve the accuracy of the computed results. Future study will include modeling of asymmetric sabot discard, which will require full 3-D computations and large computing resources.

INTENTIONALLY LEFT BLANK.

6. References

1. Schmidt, E. M., and D. D. Shear. "Aerodynamic Interference During Sabot Discard." *AIAA Journal of Spacecraft and Rockets*, vol. 15, no. 3, May–June 1978, pp. 162–167.

2. Crimi, P., and D. Siegelman. "Analysis of Mechanical and Gasdynamic Loadings During Sabot Discard From Gun-Launched Projectiles." ARBRL-CR-341, U.S. Army Ballistic Research Laboratory, Aberdeen Proving Ground, MD, June 1977.

3. Siegelman, D., J. Wang, and P. Crimi. "Computation of Sabot Discard." ARBRL-CR-505, U.S. Army Ballistic Research Laboratory, Aberdeen Proving Ground, MD, February 1983.

4. Schmidt, E. M. "Wind-Tunnel Measurements of Sabot Discard Aerodynamics." *AIAA Journal of Spacecraft and Rockets*, vol. 18, no. 3, May–June 1981, pp. 235–242.

5. Schmidt, E. M., and P. Plostins. "Aerodynamics of Asymmetric Sabot Discard." ARBRL-MR-03281, U.S. Army Ballistic Research Laboratory, Aberdeen Proving Ground, MD, June 1983.

6. Lesage, F., and B. Girard. "Wind Tunnel and CFD Investigation of Aerodynamic Interactions During Sabot Separation." AIAA Paper No. 96-0193, January 1996.

7. Nusca, M. "Computational Fluid Dynamics Application to the Aerodynamics of Symmetric Sabot Discard." AIAA Paper No. 90-3096, August 1990.

8. Nusca, M. "Numerical Simulation of Sabot Discard Aerodynamics." AIAA Paper No. 91-3255, September 1991.

9. Sahu, J. "Numerical Computations of Transonic Critical Aerodynamic Behavior." *AIAA Journal*, vol. 28, no. 5, pp. 807–816, May 1990.

10. Steger, J. L., F. C. Dougherty, and J. A. Benek. "A Chimera Grid Scheme." *Advances in Grid Generation*, edited by K. N. Ghia and U. Ghia, ASME FED-5, June 1983.

11. Benek, J. A., T. L. Donegan, and N. E. Suhs. "Extended Chimera Grid Embedding Scheme With Application to Viscous Flows." AIAA Paper No. 87-1126-CP, 1987.

12. Meakin, R. L. "Computations of the Unsteady Flow About a Generic Wing/Pylon/Finned-Store Configuration." AIAA 92-4568-CP, August 1992.

13. Sahu, J., and C. J. Nietubicz. "Application of Chimera Technique to Projectiles in Relative Motion." ARL-TR-590, U.S. Army Research Laboratory, Aberdeen Proving Ground, MD, October 1994 (also see *AIAA Journal of Spacecraft and Rockets*, vol. 32, no. 5, Sep–Oct 1995).

14. Steger, J. L., S. X. Ying, and L. B. Schiff. "A Partially Flux-Split Algorithm for Numerical Simulation of Compressible Inviscid and Viscous Flows." Proceedings of the Workshop on CFD, Institute of Nonlinear Sciences, University of California, Davis, CA, 1986.

NO. OF COPIES	ORGANIZATION
2	DEFENSE TECHNICAL INFORMATION CENTER DTIC DDA 8725 JOHN J KINGMAN RD STE 0944 FT BELVOIR VA 22060-6218
1	HQDA DAMO FDQ DENNIS SCHMIDT 400 ARMY PENTAGON WASHINGTON DC 20310-0460
1	CECOM SP & TRRSTRL COMMCTN DIV AMSEL RD ST MC M H SOICHER FT MONMOUTH NJ 07703-5203
1	PRIN DPTY FOR TCHNLGY HQ US ARMY MATCOM AMCDCG T M FISETTE 5001 EISENHOWER AVE ALEXANDRIA VA 22333-0001
1	PRIN DPTY FOR ACQUSTN HQS US ARMY MATCOM AMCDCG A D ADAMS 5001 EISENHOWER AVE ALEXANDRIA VA 22333-0001
1	DPTY CG FOR RDE HQS US ARMY MATCOM AMCRD BG BEAUCHAMP 5001 EISENHOWER AVE ALEXANDRIA VA 22333-0001
1	DPTY ASSIST SCY FOR R&T SARD TT T KILLION THE PENTAGON WASHINGTON DC 20310-0103
1	OSD OUSD(A&T)/ODDDR&E(R) J LUPO THE PENTAGON WASHINGTON DC 20301-7100

NO. OF COPIES	ORGANIZATION
1	INST FOR ADVNCD TCHNLGY THE UNIV OF TEXAS AT AUSTIN PO BOX 202797 AUSTIN TX 78720-2797
1	USAASA MOAS AI W PARRON 9325 GUNSTON RD STE N319 FT BELVOIR VA 22060-5582
1	CECOM PM GPS COL S YOUNG FT MONMOUTH NJ 07703
1	GPS JOINT PROG OFC DIR COL J CLAY 2435 VELA WAY STE 1613 LOS ANGELES AFB CA 90245-5500
1	ELECTRONIC SYS DIV DIR CECOM RDEC J NIEMELA FT MONMOUTH NJ 07703
3	DARPA L STOTTS J PENNELLA B KASPAR 3701 N FAIRFAX DR ARLINGTON VA 22203-1714
1	SPCL ASST TO WING CMNDR 50SW/CCX CAPT P H BERNSTEIN 300 O'MALLEY AVE STE 20 FALCON AFB CO 80912-3020
1	USAF SMC/CED DMA/JPO M ISON 2435 VELA WAY STE 1613 LOS ANGELES AFB CA 90245-5500
1	US MILITARY ACADEMY MATH SCI CTR OF EXCELLENCE DEPT OF MATHEMATICAL SCI MDN A MAJ DON ENGEN THAYER HALL WEST POINT NY 10996-1786

NO. OF
COPIES ORGANIZATION

1 DIRECTOR
US ARMY RESEARCH LAB
AMSRL CS AL TP
2800 POWDER MILL RD
ADELPHI MD 20783-1145

1 DIRECTOR
US ARMY RESEARCH LAB
AMSRL CS AL TA
2800 POWDER MILL RD
ADELPHI MD 20783-1145

3 DIRECTOR
US ARMY RESEARCH LAB
AMSRL CI LL
2800 POWDER MILL RD
ADELPHI MD 20783-1145

ABERDEEN PROVING GROUND

4 DIR USARL
AMSRL CI LP (305)

NO. OF
COPIES ORGANIZATION

2 USAF WRIGHT AERONAUTICAL
LABORATORIES
ATTN AFWAL FIMG
DR J SHANG
MR N E SCAGGS
WPAFB OH 45433-6553

1 COMMANDER
NAVAL SURFACE WARFARE CNTR
ATTN CODE B40 DR W YANTA
DAHLGREN, VA 22448-5100

1 COMMANDER
NAVAL SURFACE WARFARE CNTR
ATTN CODE 420 DR A WARDLAW
INDIAN HEAD, MD 20640-5035

4 DIRECTOR
NATIONAL AERONAUTICS AND
SPACE ADMINISTRATION
LANGLEY RESEARCH CENTER
ATTN TECH LIBRARY
MR D M BUSHNELL
DR M J HEMSCH
DR J SOUTH
LANGLEY STATION
HAMPTON VA 23665

2 ARPA
ATTN DR P KEMMEY
DR JAMES RICHARDSON
3701 NORTH FAIRFAX DR
ARLINGTON VA 22203-1714

7 DIRECTOR
NASA
AMES RESEARCH CENTER
ATTN MS 227 8 L SCHIFF
MS 258 1 T HOLST
MS 258 1 D CHAUSSEE
MS 258 1 M RAI
MS 258 1 P KUTLER
MS 258 1 P BUNING
MS 258 1 B MEAKIN
MOFFETT FIELD CA 94035

NO. OF
COPIES ORGANIZATION

2 USMA
DEPT OF MECHANICS
ATTN LTC ANDREW L DULL
M COSTELLO
WEST POINT NY 10996

7 COMMANDER
US ARMY ARDEC
ATTN SMCAR AET A
R DEKLEINE
C NG
R BOTTICELLI
H HUDGINS
J GRAU
S KAHN
W KOENIG
PICATINNY ARSENAL NJ 07806-5001

1 COMMANDER
US ARMY ARDEC
ATTN SMCAR CCH V
PAUL VALENTI
PICATINNY ARSENAL NJ 07806-5001

1 COMMANDER
US ARMY ARDEC
ATTN SFAE FAS SD
MIKE DEVINE
PICATINNY ARSENAL NJ 07806-5001

1 COMMANDER
US NAVAL SURFACE WEAPONS CTR
ATTN DR F MOORE
DAHLGREN VA 22448

2 UNIV OF CALIFORNIA DAVIS
DEPT OF MECHANICAL ENGG
ATTN PROF H A DWYER
PROF M HAFEZ
DAVIS CA 95616

1 AEROJET ELECTRONICS PLANT
ATTN DANIEL W PILLASCH
B170 DEPT 5311
P O BOX 296
1100 WEST HOLLYVALE STREET
AZUSA CA 91702

NO. OF
COPIES ORGANIZATION

3 SCIENCE AND TECHNOLOGY INC
4001 NORTH FAIRFAX DR NO 700
ATTN DR ALAN GLASSER
MR BRUCE LOHMAN
MR DAVE MAURIZI
ARLINGTON VA 22203-1618

3 AIR FORCE ARMAMENT LAB
ATTN AFATL/FXA
STEPHEN C KORN
BRUCE SIMPSON
DAVE BELK
EGLIN AFB FL 32542-5434

1 MASSACHUSETTS INSTITUTE OF TECHNOLOGY
ATTN TECH LIBRARY
77 MASSACHUSETTS AVE
CAMBRIDGE MA 02139

1 GRUMANN AEROSPACE CORPORATION
AEROPHYSICS RESEARCH DEPT
ATTN DR R E MELNIK
BETHPAGE NY 11714

2 MICRO CRAFT INC
ATTN DR JOHN BENEK
NORMAN SUHS
207 BIG SPRINGS AVE
TULLAHOMA TN 37388-0370

1 LOS ALAMOS NATIONAL LAB
ATTN MR BILL HOGAN
MS G770
LOS ALAMOS NM 87545

3 DIRECTOR
SANDIA NATIONAL LABORATORIES
ATTN DIV 1554 DR W OBERKAMPF
DIV 1554 DR F BLOTTNER
DIV 1636 DR W WOLFE
ALBUQUERQUE NM 87185

1 NAVAL AIR WARFARE CENTER
ATTN DAVID FINDLAY
MS 3 BLDG 2187
PATUXENT RIVER MD 20670

NO. OF
COPIES ORGANIZATION

1 METACOMP TECHNOLOGIES INC
ATTN S R CHAKRAVARTHY
650 HAMPSHIRE ROAD
SUITE 200
WESTLAKE VILLAGE CA 91361-2510

2 ROCKWELL SCIENCE CENTER
ATTN S V RAMAKRISHNAN
V V SHANKAR
1049 CAMINO DOS RIOS
THOUSAND OAKS CA 91360

1 ADVANCED TECHNOLOGY CTR
ARVIN/CALSPAN
AERODYNAMICS RESEARCH DEPT
ATTN DR M S HOLDEN
PO BOX 400
BUFFALO NY 14225

1 PENNSYLVANIA STATE UNIV
DEPT OF AEROSPACE ENGG
ATTN DR G S DULIKRAVICH
UNIVERSITY PARK PA 16802

1 UNIV OF ILLINOIS AT URBANA CHAMPAIGN
DEPT OF MECHANICAL AND INDUSTRIAL ENGINEERING
ATTN DR J C DUTTON
URBANA IL 61801

1 UNIVERSITY OF MARYLAND
DEPT OF AEROSPACE ENGG
ATTN DR J D ANDERSON JR
COLLEGE PARK MD 20742

1 UNIVERSITY OF NOTRE DAME
DEPT OF AERONAUTICAL AND MECHANICAL ENGINEERING
ATTN PROF T J MUELLER
NOTRE DAME IN 46556

1 UNIVERSITY OF TEXAS
DEPT OF AEROSPACE ENGG MECHANICS
ATTN DR D S DOLLING
AUSTIN TX 78712-1055

1 UNIVERSITY OF DELAWARE
DEPT OF MECHANICAL ENGG
ATTN DR JOHN MEAKIN
NEWARK DE 19716

1 UNIVERSITY OF FLORIDA
DEPT OF ENGG SCIENCES
COLLEGE OF ENGINEERING
ATTN PROF C C HSU
GAINESVILLE FL 32611

ABERDEEN PROVING GROUND

27 DIR USARL
ATTN AMSRL-WM-P
A HORST
E SCHMIDT
AMSRL-WM-PB
P PLOSTINS
D LYON
M BUNDY
K FANSLER
E FERRY
B GUIDOS
K HEAVEY
H EDGE
V OSKAY
A MIKHAIL
J SAHU
P WEINACHT
AMSRL-ST, J ROCCHIO
AMSRL-WM-PD, B BURNS
AMSRL-WM-PA
G KELLER
M NUSCA
AMSRL-WM-PC, B FORCH
AMSRL-WM-W, C MURPHY
AMSRL-WM-WB, W D'AMICO
AMSRL-WM-TB, R LOTTERO
AMSRL-CI-H
C NIETUBICZ
AMSRL-CI-HC
P COLLINS
D HISLEY
D PRESSEL
W STUREK

2 CDR ARDEC
ATTN FIRING TABLES, BLDG 120
R LIESKE
R EITMILLER

INTENTIONALLY LEFT BLANK.

REPORT DOCUMENTATION PAGE

Form Approved OMB No. 0704-0188

1. AGENCY USE ONLY *(Leave blank)*	2. REPORT DATE	3. REPORT TYPE AND DATES COVERED
	October 1997	Final, Oct 95 - Sep 96

4. TITLE AND SUBTITLE
Navier-Stokes Computations of Sabot Discard Using Chimera Scheme

5. FUNDING NUMBERS
1L161102AH43

6. AUTHOR(S)
E. Ferry, J. Sahu, and K. Heavey

7. PERFORMING ORGANIZATION NAME(S) AND ADDRESS(ES)
U.S. Army Research Laboratory
ATTN: AMSRL-WM-PB
Aberdeen Proving Ground, MD 21005-5066

8. PERFORMING ORGANIZATION REPORT NUMBER
ARL-TR-1524

9. SPONSORING/MONITORING AGENCY NAMES(S) AND ADDRESS(ES)

10.SPONSORING/MONITORING AGENCY REPORT NUMBER

11. SUPPLEMENTARY NOTES

12a. DISTRIBUTION/AVAILABILITY STATEMENT
Approved for public release; distribution is unlimited.

12b. DISTRIBUTION CODE

13. ABSTRACT *(Maximum 200 words)*

Computational fluid dynamics calculations have been performed for a multibody system consisting of a main projectile and three sabot components. Numerical flow field computations have been made for various orientations and locations of sabots using an unsteady, zonal Navier-Stokes code and the Chimera composite grid discretization technique at $M_\infty = 4.0$ and $\alpha = 0°$. Computational grids have been obtained for the projectile and sabot independently and then overset to form the complete grid system. Computed results have been obtained for sabot angles of attack of 5, 10, 15, and 25°. Computed results show the details of the expected flow field features including the shock interactions. Both laminar and turbulent computations for the 25° case predict similar results. Computed results for other sabot positions are compared with the experimental data obtained in Canada for the same configuration and conditions and are generally found to be in good agreement with the data.

14. SUBJECT TERMS
kinetic energy projectiles, sabot discard, Navier-Stokes equations, Chimera composite grid technique, steady-state numerical calculations, shock interaction, pressure contours, surface pressure distribution

15. NUMBER OF PAGES
25

16. PRICE CODE

17. SECURITY CLASSIFICATION OF REPORT	18. SECURITY CLASSIFICATION OF THIS PAGE	19. SECURITY CLASSIFICATION OF ABSTRACT	20. LIMITATION OF ABSTRACT
UNCLASSIFIED	UNCLASSIFIED	UNCLASSIFIED	UL

NSN 7540-01-280-5500

Standard Form 298 (Rev. 2-89)
Prescribed by ANSI Std. 239-18 298-102

INTENTIONALLY LEFT BLANK.

USER EVALUATION SHEET/CHANGE OF ADDRESS

This Laboratory undertakes a continuing effort to improve the quality of the reports it publishes. Your comments/answers to the items/questions below will aid us in our efforts.

1. ARL Report Number/Author ARL-TR-1524 (Ferry) Date of Report October 1997

2. Date Report Received _____

3. Does this report satisfy a need? (Comment on purpose, related project, or other area of interest for which the report will be used.) _____

4. Specifically, how is the report being used? (Information source, design data, procedure, source of ideas, etc.) _____

5. Has the information in this report led to any quantitative savings as far as man-hours or dollars saved, operating costs avoided, or efficiencies achieved, etc? If so, please elaborate. _____

6. General Comments. What do you think should be changed to improve future reports? (Indicate changes to organization, technical content, format, etc.) _____

CURRENT ADDRESS

Organization

Name E-mail Name

Street or P.O. Box No.

City, State, Zip Code

7. If indicating a Change of Address or Address Correction, please provide the Current or Correct address above and the Old or Incorrect address below.

OLD ADDRESS

Organization

Name

Street or P.O. Box No.

City, State, Zip Code

(Remove this sheet, fold as indicated, tape closed, and mail.)

(DO NOT STAPLE)

DEPARTMENT OF THE ARMY

OFFICIAL BUSINESS

NO POSTAGE
NECESSARY
IF MAILED
IN THE
UNITED STATES

BUSINESS REPLY MAIL
FIRST CLASS PERMIT NO 0001,APG,MD

POSTAGE WILL BE PAID BY ADDRESSEE

DIRECTOR
US ARMY RESEARCH LABORATORY
ATTN AMSRL WM PB
ABERDEEN PROVING GROUND MD 21005-5066